

Multifunctional molecular imaging probes for estrogen receptors: ^{99m}Tc labeled diethylstilbestrol (DES) conjugated, cuinp quantum dot nanoparticles (DESCIP)

Payam Moharrami¹ · Perihan Unak¹ · Ozge Kozguş Guldu¹ · E. İ. Medine¹ · Gul Gumuser² · Elvan Sayıt Bilgin² · Omer Aras³

Received: 7 August 2017 / Published online: 11 November 2017
© Akadémiai Kiadó, Budapest, Hungary 2017

Abstract A theranostic nanoparticle was synthesized based on diethylstilbestrol conjugated with phosphate, copper, and indium (DESCIP) and labelled with ^{99m}Tc which can be used for SPECT imaging of ER-enriched cancers. In vitro biological activity of ^{99m}Tc -DESCIP was examined in breast adenocarcinoma cells (MCF-7), prostatic carcinoma cells (PC-3), and pulmonary epithelial cells (A-549). In vivo lymph node imaging was performed in normal and receptor blocked female New Zealand rabbits. Results demonstrated that ^{99m}Tc -DESCIP and DESCIP has potential for imaging ER-enriched tumors such as breast and prostate tumors, and their metastases in the lung, as well as improving management for their therapies.

Keywords Diethylstilbestrol · Quantum dot nanoparticles · Cancer imaging · Breast cancer · Prostate cancer · Lung cancer

Electronic supplementary material The online version of this article (<https://doi.org/10.1007/s10967-017-5630-2>) contains supplementary material, which is available to authorized users.

✉ Perihan Unak
perihan.unak@gmail.com

¹ Department of Nuclear Applications, Ege University, Institute of Nuclear Sciences, 35100 Bornova Izmir, Turkey

² Department of Nuclear Medicine, Celal Bayar University, Manisa, Turkey

³ Department of Radiology, Mem Sloan Kettering Cancer Center, 1275 York Ave, New York, NY 10065, USA

Introduction

Fluorescence-based detection is the most common method utilized in biosensing because of its high sensitivity, simplicity, and diversity. In the era of nanotechnology, nanomaterials are starting to replace traditional organic dyes as detection labels because they offer superior optical properties, such as brighter fluorescence, wider selections of excitation and emission wavelengths, higher photostability, etc. Their size- or shape-controllable optical characteristics also facilitate the selection of diverse probes for higher assay throughput. Furthermore, the nanostructure can provide a solid support for sensing assays with multiple probe molecules attached to each nanostructure, simplifying assay design and increasing the labelling ratio for higher sensitivity.

Cell imaging using fluorescence dye can supply detailed anatomic information of the cancerous cell or tissue. Consequently, it is used for both clinical and research purposes. Quantum dot nanoparticles present a promising alternative. They can be easily prepared using II-VI elements (such as CdS, CdSe, CdTe, ZnS, ZnSe, CuInP, InP, etc.) that are dissolved in various organic solvents or in aqueous media at appropriate conditions. They not only have a tendency to bioconjugate but also demonstrate fluorescence properties. Because of their semiconductor properties, they have multiple uses in other areas of technology besides medical imaging.

The major endocrine-related cancers in humans display gender-specific hormonal responsiveness. In women, estrogen plays an important role in breast and endometrial cancer, and in men, androgen plays an important role in prostate cancer [1–6]. Two types of estrogen receptors have been classified: ER- α and ER- β . The treatment strategy depends on whether the receptors are positive or negative

[7–10]. For example, estrogen receptor-blocking drugs such as tamoxifen have been used to treat ER α -positive tumors [4, 5].

Diethylstilbestrol (DES), a nonsteroidal estrogen, was first synthesized in 1938 [1]. It was the first synthetic estrogen to be made and was occasionally prescribed for the treatment of advanced breast and prostate cancer [2, 3]. A well-known teratogen and carcinogen, DES inhibits the hypothalamic–pituitary–gonadal axis, consequently blocking the testicular synthesis of testosterone, lowering plasma testosterone, and inducing a chemical castration [2, 3, 6]. Recently, we synthesized a phosphate derivative of diethylstilbestrol (DESP) and labelled it with ^{99m}Tc to study its imaging potential [11]. DESP is the diphosphate ester of a synthetic, nonsteroidal form of estrogen (Fosfestrol; Diethylstilbestrol diphosphate; Phosphestrol) [12].

The main objective of this work is to determine the potential of DES conjugated with phosphate-, copper-, and indium-nanoparticles (DESCIP) and labelled with ^{99m}Tc for targeting and detecting estrogen receptor-enriched cancer cells. By adding phosphorus-, copper- and indium-containing nanoparticles to the DES structure, we conferred multimodality imaging capability (single-photon emission computed tomography and fluorescence). In vitro cell labeling and in vivo lymph node imaging properties were determined. Figure 1 shows a schematic representation of DESCIP distribution in cancer cells.

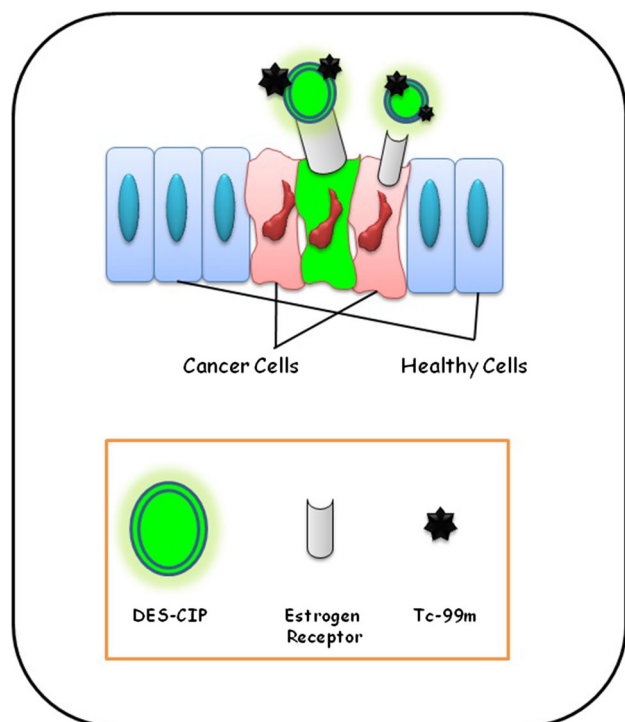


Fig. 1 Schema for DESCIP distribution in cancerous cells

Experimental

Equipment and sources of material

$\text{Na}^{99m}\text{TcO}_4$ was supplied by the Sifa University of Izmir/Turkey. DES was purchased from Sigma. All other chemicals were supplied from Merck Chemical Co., (Darmstadt Germany) and Aldrich Chemical Co., (Germany). Breast adenocarcinoma cells (MCF-7), prostate carcinoma cells (PC-3), and pulmonary epithelial cells (A-549) were supplied from the American Type Culture Collection (Manassas, VA USA).

The following equipment from Ege University Institute of Nuclear Sciences were used: Cd (Te) detector equipped with a thin layer radio chromatography (TLRC); high-performance liquid chromatography (Shimadzu Corporation, Somerset, NJ, USA) equipped with a LC-10ATvp quaternary pump, SIL-20A HT auto sampler, and 7.0 μm reversed-phase-C-18 column 250 \times 21 mm I.D. (Macherey–Nagel, Bethlehem, PA, USA); and Perkin Elmer Optima 2000 DV (to produce Inductively Coupled Plasma OES (ICP-OES) chromatograms). The Institute of Technology, Izmir provided X-ray powder diffraction (XRD) analyses using the Philips X'Pert Pro (Phillips, Amsterdam, Netherlands), imaging using the Philips XL-30 FEG Scanning Electron Microscope (SEM) (Phillips, Amsterdam, Netherlands), and size analyses in liquid ambience chromatograms using a Zetasizer. Fourier Transform Infrared Spectra (FTIR) spectra were obtained from the Celal Bayar University. Nuclear magnetic resonance (NMR) chromatograms were obtained from Ataturk University.

Synthesis of DESCIP

26.8 mg (0.1 mmol) of DES was dissolved in 4 mL pyridine using a magnetic stirrer. Then, 24.5 mg (0.2 mmol) of copper(I)acetate, 44.2 mg (0.2 mmol) of indium(III)chloride, and 100 μl of POCl_3 were added drop-wise. The mixture was stirred for 24 h at room temperature. After the reaction completed and pyridine evaporated, the product was washed with 10 mL of dichloromethane and 10 mL of distilled water. The product was rewashed with 10 mL of dichloromethane and 10 mL of distilled water. It was centrifuged 10 min at 2500 rpm. Then, the upper (aqueous) phase was separated and the pH was adjusted to 9 using 3 M LiOH solution. The mixture was re-centrifuged for 10 min at 2500 RPM and the upper (aqueous) phase was eluted using with Dowex 50 anion exchange column. The eluate was stored at 4 $^\circ\text{C}$.

Structural analysis of DESCIP

Inductively coupled plasma mass spectrometry (ICP-MS)

ICP analyses were conducted in order to understand the elemental composition of DESCIP. Standard solutions of copper, indium, and phosphorous were used to determine the elemental composition of DESCIP nanoparticles. 100 $\mu\text{L}/\mu\text{g}$ of DESCIP solution was used for the analyses.

Fourier transform infrared spectra (FTIR) and nuclear magnetic resonance (NMR)

10 mg of lyophilized DESCIP were mixed thoroughly with 100 mg of anhydrous KBr in a mortar while grinding with the pestle; the pellet was prepared for the acquisition of FTIR spectra. ^1H -NMR and ^{13}C -NMR spectra were acquired to identify molecular structures (Fig. 2). CDCl_3 was used as solvent. Theoretical (ACD/LogP Algorithm) spectra were used for comparison with experimental NMR spectra.

Characterization of DESCIP

The mean particle size was determined by dynamic light scattering and the surface charge of the nanoparticles was investigated through zeta potential measurements after dilution in ethanol (Fig. 3). The particle size and morphology of DESCIP were assessed by SEM (Fig. 4).

The nanoparticles were analyzed by XRD, $\text{Cu K}\alpha$ ($\lambda = 1.541 \text{ \AA}$) radiation wavelength at 40 kV and 40 mA. The samples were scanned between 0° and 80° .

Fluorescence spectra of DESCIP

1 mg/mL of DESCIP was prepared in ethanol. The fluorescence spectra were acquired at 250 nm excitation and 450 nm emission wavelengths.

$^{99\text{m}}\text{Tc}$ labeling of DESCIP

Stock solutions of DESCIP (1.19 mg/0.2 mL distilled water) and SnCl_2 (1 mg/1 mL distilled water) were prepared. Then, 50 μL of DESCIP and 100 μL of SnCl_2 were mixed in a tube at a pH of 7. 1 mCi (37 MBq) of $^{99\text{m}}\text{TcO}_4$ was added to the mixture and the resulting product was incubated for 20 min at room temperature. Rf value and radiolabeling yield of $^{99\text{m}}\text{Tc}$ labeled DESCIP ($^{99\text{m}}\text{Tc}$ -DESCIP) were determined by TLRC.

Quality control studies of $^{99\text{m}}\text{Tc}$ -DESCIP

Thin layer radio chromatography (TLRC)

The same procedure as in our previous reports was applied to obtain TLRC chromatograms (mobile phase: acid citrate dextrose and physiological serum (0.90% NaCl)). TLRC chromatograms were acquired using a Bioscan AR-2000

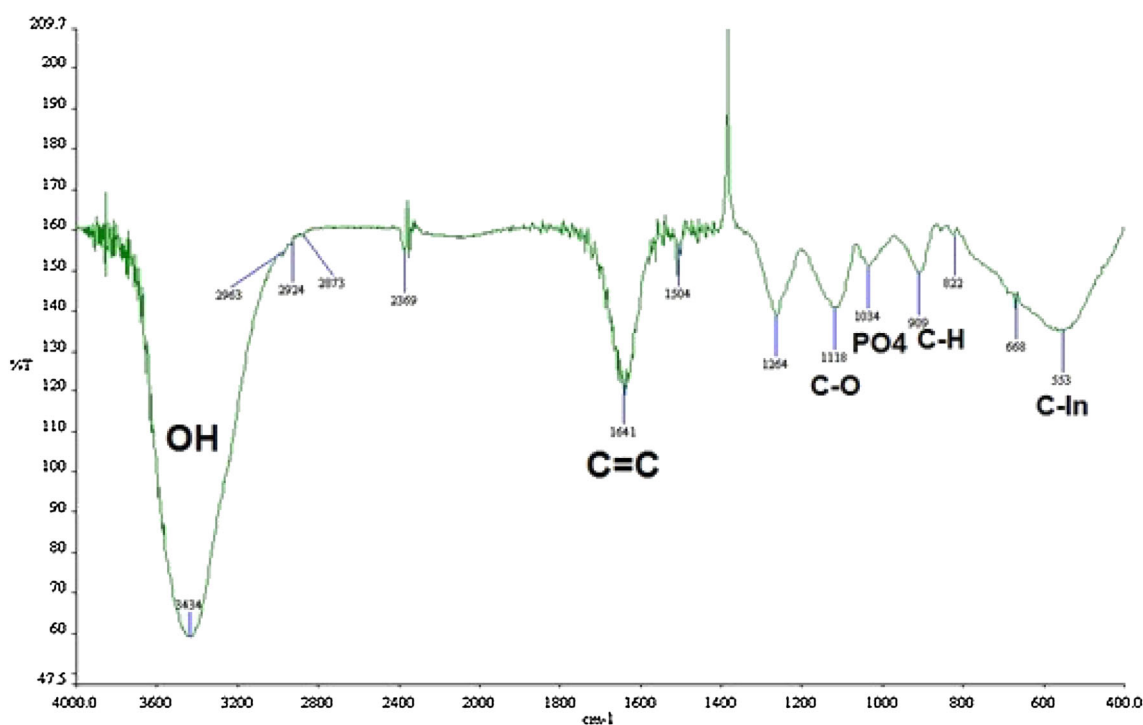


Fig. 2 FTIR spectra of DESCIP nanoparticles

Fig. 3 Hydrodynamic size distribution of the DESCIP nanoparticles

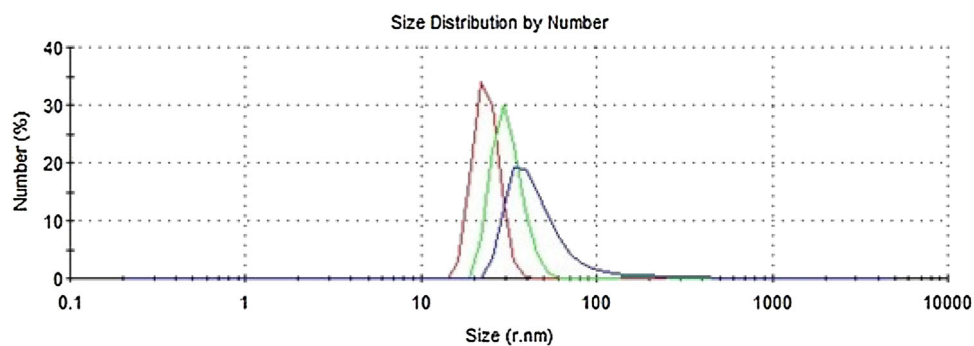
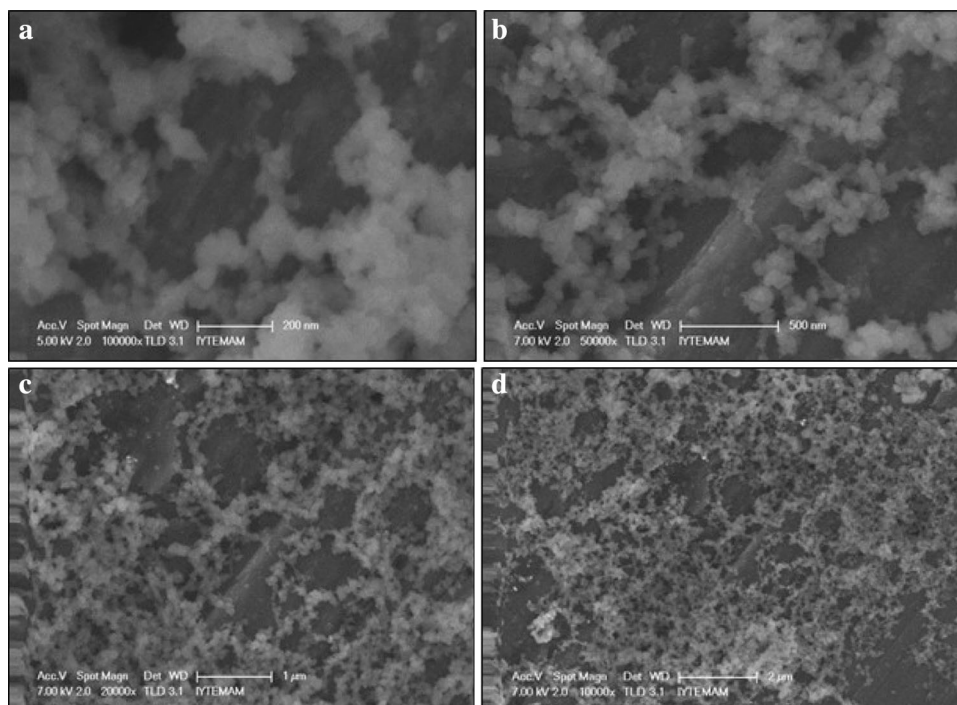


Fig. 4 SEM images of DESCIP nanoparticles: **a** 200nm, **b** 500nm, **c** 1 μ m, and **d** 2 μ m



Scanner. Rf values of each component were determined. Table 1 presents Rf values of $^{99m}\text{TcO}_4^-$, Reduced ^{99m}Tc and $^{99m}\text{Tc-DESCIP}$.

Stability testing

To perform stability tests of the radiolabeling, 50 $\mu\text{g}/50 \mu\text{L}$ aliquots of $^{99m}\text{Tc-DESCIP}$ were incubated in physiological

Table 1 Rf values of $^{99m}\text{TcO}_4^-$, Reduced ^{99m}Tc and $^{99m}\text{Tc-DESCIP}$

TLRC solvent	$^{99m}\text{TcO}_4^-$	Red. ^{99m}Tc	$^{99m}\text{Tc-DES-P/Cu/In}$
Mobile phase 1*	0.91	0.034	0.92
Mobile phase 1*	0.941	0.054	0.047

*Mobile phase 1: Acid Citrate Dextrose (ACD); Mobile phase 2: Physiological serum (0.90% NaCl)

serum at 37 °C in a humidified 5% CO_2 incubator. Then, they were analyzed using RTLC at several time intervals to determine if there is any impurity up to 4 h during the observation period.

Lipophilicity studies

Lipophilicities were determined similar to our previous reports [13, 14]. Briefly, 100 μL aliquots of $^{99m}\text{Tc-DESCIP}$ were put into a test tube together with 300 μL of n-octanol and 300 μL of PBS volumes. Subsequently, the mixture was vortexed for 1 min at room temperature and centrifuged at 2500 rpm for 30 min. Then, the radioactivities of the top and bottom phases were counted. The partition coefficient (LogP) was determined by dividing the counts in the n-octanol layer with the counts in the aqueous layer.

In vitro Bioaffinities of ^{99m}Tc -DESCIP

In vitro bioaffinities of ^{99m}Tc -DESCIP were examined in breast adenocarcinoma (MCF-7), prostate carcinoma (PC-3), and pulmonary epithelial (A-549) cell lines. Cells were cultured in DMEM, 10% FBS (Fetal Bovine Serum), 1% PSS, (100 units/ml penicillin and 100 $\mu\text{g}/\text{ml}$ streptomycin), 1% L-Glutamine, 2% NaHCO_3 , 1% sodium pyruvate, 1% non-essential amino acid mixture in cell culture flasks. After cells have proliferated enough to cover 80% of the flasks, they were separated from the surface using 0.25% (w/v) trypsin–EDTA solution and distributed into 24-well plates (500 μl for each well). Time-dependent incorporation ratios were then examined in ER positive (+) and ER negative (–) cells.

Cell incorporation study with receptor unblocked ER negative (–) cells

10 μg (4 MBq/ μg) of ^{99m}Tc -DESCIP was added to 5 mL of culture medium and the resulting solution was administered upon the cells in the 24-well plates. At 30, 60, and 120 min following administration, the radioactivity in the cells were counted with Cd(Te) semi-conductor detector (A0). Then, they were washed by RIPA buffer for three times and the counts were read for second (A1) time (Table 2) (Fig. 7).

Cell incorporation study with receptor blocked ER positive (\pm) cells

In order to determine receptor saturation, 1.2 mg ^{99m}Tc -DESCIP was dissolved in 20 μl ethanol, and then it was put into 5 ml culture medium and incubated with the cells for 2 h. Following that, the study continued similar to that for ER (–) cells (Table 3) (Fig. 7).

Fluorescence imaging studies of DESCIP

In order to obtain fluorescence images, cells (MCF-7, PC-3 and A-549) were cultured and prepared on chamber slide plates. Then, 200 μl of DESCIP was applied to cells and fluorescence imaging was obtained using the fluorescence

microscope at 20X and 40X magnification over 4 h (Fig. 8).

For comparison, DESP labelled with FITC (fluorescein isothiocyanate) (FITC), a common fluorescence dye, was also prepared. For FITC labeling, 1 mg of DESP solution was prepared in 1 mL of 0.1 M sodium carbonate buffer (pH 9). Then, 1 mg of FITC was dissolved in 1 mL of anhydrous DMSO. 50 μL of the FITC solution was added to the DESP solution very slowly in 5 μL aliquots and continuously stirred. The obtained solution was incubated for 8 h at 4 $^\circ\text{C}$ in the dark. 50 mM of NH_4Cl was added to the solution and it was incubated for 2 more hours at 4 $^\circ\text{C}$. Finally, unbound FITC was separated from the conjugate by gel filtration using Sephadex G-25 column. MCF-7, PC-3 and A-549 cells cultured on chamber slides were washed with PBS and the medium with FITC-labeled DESP was added to the cells. After a 4 h incubation time, cells were washed with PBS ($\times 2$) and imaging was acquired using fluorescence microscopy with a green filter (520 nm) (Fig. 9).

All fluorescence imaging studies were performed in dark conditions.

Cytotoxicities

The MTT assay procedure was applied similar to our previous reports [14, 15]. The cells (MCF-7, PC-3, and A-549) were sustained in minimal essential medium and were prepared from confluent monolayer cultures and plated at a density of 8×10^3 cells in a 96-well plate. The incubation conditions were 48 h at 37 $^\circ\text{C}$. Stock solutions of DESCIP and DES (1, 2, 3, 4 ng/mL) were prepared by dissolving them in PBS. Appropriate dilutions of the samples were prepared in growth medium and added to the cells. The resulting mixture was incubated for 24, 48, and 72 h. After each incubation period, viable cells were determined using MTT.

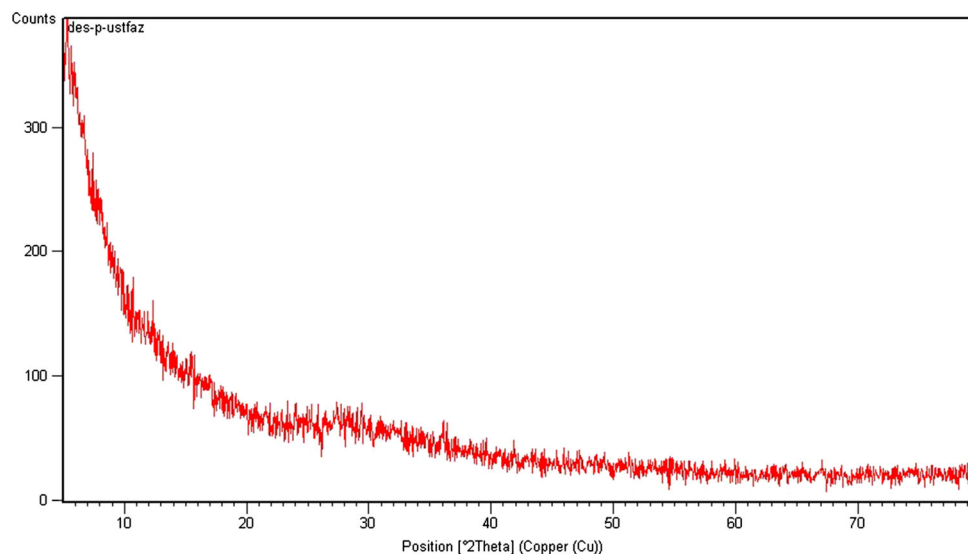
The absorbance was measured on a Varioscan microplate reader (Thermo, USA) at 520 nm. The intensity of color is directly proportional to the percentage of viable cells. Tests were carried out in quadruplicate and each experiment was repeated six times.

Table 2 Incorporation ratios (%) for receptor unblocked [ER(–)] cells

Incubation period (min)	DESCIP			^{99m}Tc		
	MCF-7	PC-3	A-549	MCF-7	PC-3	A-549
30	5.2 \pm 2.4	2.4 \pm 1.2	2 \pm 0.7	0.1 \pm 0.1	0.2 \pm 0.1	0.2 \pm 0
60	8.1 \pm 1.8	3.3 \pm 1.1	1.9 \pm 0.6	0 \pm 0	0.1 \pm 0.1	0.2 \pm 0
120	19.8 \pm 4.5	8.7 \pm 3.5	4.2 \pm 1.3	0.2 \pm 0.1	0 \pm 0	0.1 \pm 0.1

Table 3 Incorporation ratios (%) for receptor blocked [ER(+)] cells

Incubation period (min)	DES-P/Cu/In			^{99m} Tc		
	MCF-7	PC-3	A-549	MCF-7	PC-3	A-549
30	0.9 ± 0.7	0.5 ± 0.1	0.2 ± 0.1	0.1 ± 0.1	0.2 ± 0.1	0.2 ± 0.1
60	1.4 ± 1.3	0.6 ± 0.2	0.2 ± 0.1	0.1 ± 0.1	0.1 ± 0.1	0.1 ± 0.1
120	1.6 ± 0.8	1 ± 0.7	0.2 ± 0.1	0 ± 0	0.2 ± 0.1	0.1 ± 0

Fig. 5 X-ray diffraction (XRD) pattern of DESCIP nanoparticles

Sentinel lymph node imaging studies in rabbits

Static imaging and dynamic imaging were performed using a gamma camera (Diacan Instruments) in Celal Bayar University, School of Medicine, Department of Nuclear Medicine. All procedures were approved by the Animal Ethics Committee at Ege University. Eight normal and eight receptor blocked female New Zealand white rabbits (weight 2.5–3.0 kg) were used in the study. A cocktail 3 mL of Ketamine (50 mg/kg)/xylazine (10 mg/kg) anesthetic was injected intramuscularly in the brachial muscle. The hair on the medial side of the distal hind limb was shaved. ^{99m}Tc-DESCIP (7.4 Mbq/10.8 mg/0.1 ml per rabbit) nanoparticles were injected intradermally into the distal hind limb. Receptor saturation was supplied as previously by using DES [11]. 1.2 mg of DES was dissolved in 20 µL of ethanol then diluted with 15 mL of physiological serum. 10 g of DES was taken and used for receptor saturation 15 min prior to ^{99m}Tc-DESCIP injection.

Dynamic (64 × 64 matrix, 1 zoom) and static (256 × 256 matrix, 1 zoom) lymphoscintigraphic images were taken up to 24 h. Fifteen dynamic images (each for 20 s) and 5 min static images (at 5th, 15th, 30th, 60th, 120th min and 24 h) were obtained in the supine position (Fig. 10).

Statistical analysis

One-way analysis of variance and non-linear regression was conducted using the GraphPad software (GraphPad Software, Inc, San Diego, CA). Statistical differences were considered significant at $p < 0.05$.

Results and discussion

Proposed structure of DESCIP

FTIR spectra of DESCIP showed OH stretch at 3434 nm; C=C stretch at 1641 nm; C–O stretch at 1118 nm; P–O stretch at 1034 nm; C–H stretch at 909 nm; and C–In stretch at 553 nm (Fig. 2).

¹H-NMR and ¹³C-NMR spectra of DESCIP verified that the estrogen ring in the structure is protected; main peaks were 1 ppm (21 and 23 numbered aliphatic methyl groups); 2–3 ppm (20 and 22 numbered CH₂ groups); 5 ppm (OH protons); and 7 ppm (aromatic ring protons).

¹³C-NMR spectra presented main peaks of 10–20 ppm for methyl carbons; 30 ppm for CH₂ groups; 120, 150 ppm for aromatic ring carbons; and 136 ppm for methylene carbons (supplementary data).

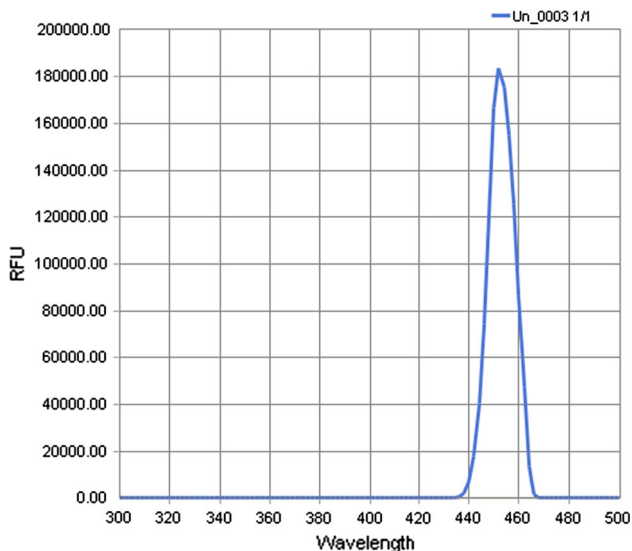


Fig. 6 Fluorescence spectra of DESCIP nanoparticles

Elemental ratios were found to be $In_2Cu_5P_7$ according to ICP analyses

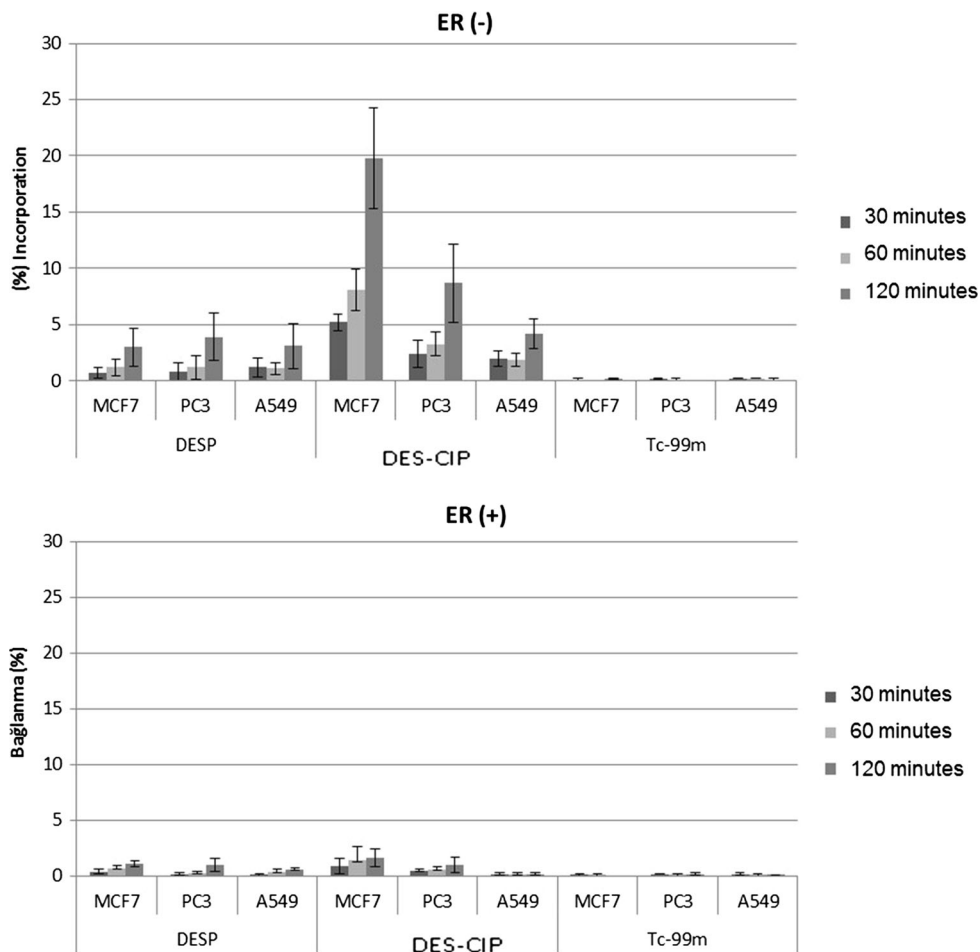
Lastly, fluorescence spectra showed green fluorescence (Fig. 6). The excitation wavelength was 250 nm and the emission wavelength was 450 nm. NMR, FTIR, and ICP analyses confirmed that the estrogen ring was existent in the structure and atomic ratios was 5/2/7 for copper, indium, and phosphorous.

Characterization of DESCIP

X-ray diffraction was used for characterization of nano-materials. Although there were no data for CuInP nanoparticles, our results confirmed characteristic diffraction peaks for Cu, In, and P (Fig. 5). The characterization of the structures was verified by crystal characteristics of the face centered cubic structure.

SEM images determined that the size of DESCIP nanoparticles were about 10–20 nm (Fig. 4) while hydrodynamic diameters of DESCIP nanoparticles were about

Fig. 7 Incorporation ratios for ER unblocked [ER(-)] and ER blocked [ER(+)] cells



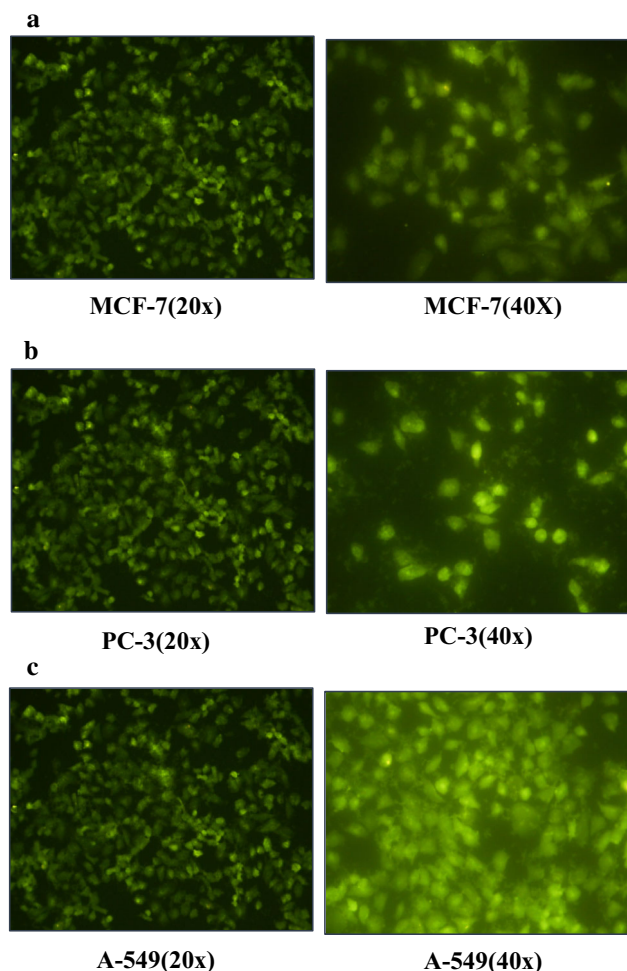


Fig. 8 Fluorescence images of DESCIP incorporated **a** MCF-7 cells (20×, 40× enlarged); **b** PC-3 cells (20×, 40× enlarged); **c** A-549 cells (20×, 40× enlarged)

50 nm (Fig. 3). Additionally, DESCIP nanoparticles were shown to have stable green fluorescence at 450 nm (350 nm excitation) (Fig. 6).

Quality control studies showed that DESCIP nanoparticles were successfully labelled with ^{99m}Tc , with a 99% labeling yield using SnCl_2 as a reducing agent, and stability was established for at least 4 h at room temperature. R_f values of $^{99m}\text{TcO}_4^-$, reduced ^{99m}Tc and ^{99m}Tc -DESCIP are presented in Table 1. Both DESP and DESCIP can be labeled with ^{99m}Tc by direct labeling using SnCl_2 as reducing agent. ^{99m}Tc can be attached to DESCIP through P and O atoms similar mechanism with DESP [11] and methylenediphosphonate [16] which have been used as bone imaging agent.

The lipophilicities of ^{99m}Tc -DESP and ^{99m}Tc -DESCIP were found to be -2.0 ± 0.01 , and -1.23 ± 0.20 , respectively.

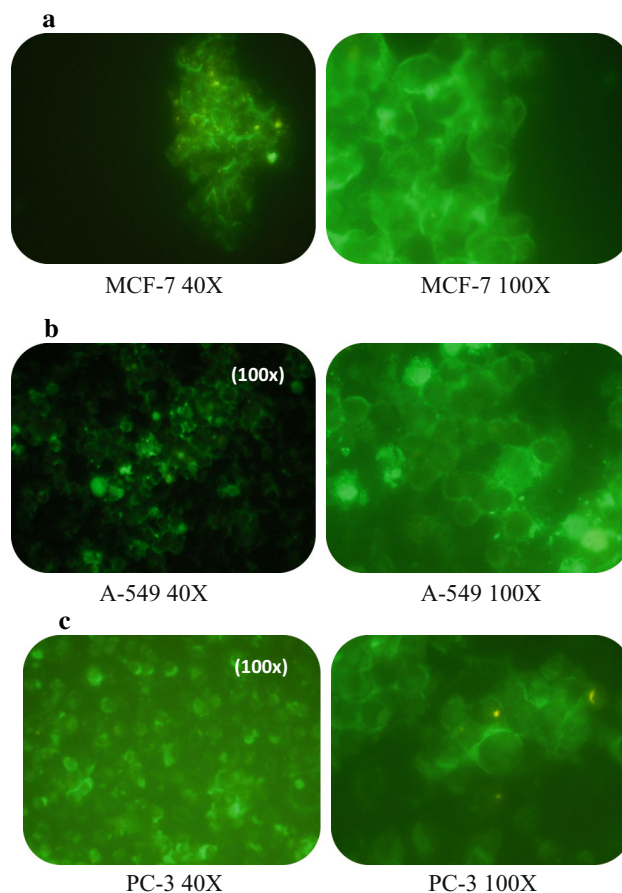


Fig. 9 Fluorescence images of FITC labeled DESP incorporated cells **a** MCF-7 cells (40×, 100× enlarged); **b** A-549 cells (40×, 100× enlarged); **c** PC-3 cells (40×, 100× enlarged)

In vitro incorporation results

According to time-dependent in vitro incorporation results (Fig. 7, Tables 2, 3), ^{99m}Tc -DESCIP or ^{99m}Tc -DESP both showed higher uptake in every cell line than $^{99m}\text{TcO}_4^-$ as a control group ($p < 0.05$). The highest incorporation ratio was observed in the MCF-7 cell line and the lowest in the A-549 cell line. Estrogen plays an important role not only in the development of normal mammary glands, but also in the proliferation and progression of breast cancer. There are two types of estrogen receptors: $\text{ER}\alpha$ and $\text{ER}\beta$ which was first reported in 1996 [17, 18]. The MCF-7 cell line is one of the most frequently used cell lines for functional observation of estrogen response and represents an $\text{ER}\alpha$ -positive breast cancer cell line [19, 20]. On the other hand, the prostate is known as an androgen target; however, it is also targeted for estrogen. Recent studies have shown that estrogens, in combination with androgens, play critical roles in prostate carcinogenesis [21–23]. Moreover, $\text{ER}\alpha$ is also present in prostate stromal cells of normal, hyperplastic, and cancerous prostate tissue [23–26]. There are

Table 4 Cellular cytotoxicity of DESP in 24, 48 and 72 h for MCF7, PC3 and A549 cells

24th h			
Log kons (ng/mL)	MCF7	PC3	A549
0	91.54 ± 2.56	96.45 ± 3.84	95.78 ± 4.32
1	95.23 ± 3.44	92.77 ± 3.39	94.5 ± 4.88
2	96.58 ± 3.78	95.67 ± 4.14	97.21 ± 3.65
3	93.49 ± 2.99	94.64 ± 4.66	93.56 ± 3.98
4	97.33 ± 3.76	93.89 ± 4.28	96.58 ± 2.98
48th h			
Log kons (ng/mL)	MCF7	PC3	A549
0	92.48 ± 3.42	93.8 ± 2.34	96.44 ± 3.44
1	94.37 ± 2.59	94.43 ± 3.56	93.21 ± 3.78
2	91.4 ± 3.66	97.32 ± 4.21	98.43 ± 3.21
3	95.32 ± 2.78	94.71 ± 3.98	95.88 ± 4.56
4	93.44 ± 4.32	96.19 ± 3.74	96.83 ± 4.33
72th h			
Log kons (ng/mL)	MCF7	PC3	A549
0	97.34 ± 2.32	94.3 ± 3.45	95.97 ± 4.31
1	96.03 ± 3.21	95.87 ± 2.89	91.68 ± 3.76
2	97.48 ± 2.78	91.45 ± 3.46	97.3 ± 2.91
3	95.39 ± 3.45	98.21 ± 2.78	93.78 ± 3.56
4	98.29 ± 4.57	92 ± 4.12	97.34 ± 2.83

some reports indicating a possible role of ER α in promoting inflammation, proliferation, and metastasis in prostate cancer [27, 28] and thus ER receptor targeting can be considered as a potential target for prostate cancer prevention therapy [29, 30]. Lastly, although estrogen receptors are highly expressed in breast cancer tissue, there are also some reports indicating estrogen receptors (ER α and ER β) expression in normal lung tissue and small cell lung cancer tissue [31–33]. Our results show that we achieved the highest incorporation ratios on ER (+) positive MCF breast cancer cells, followed by PC-3 prostate cancer cells, and then A-549 lung cancer cells. Therefore, we propose that incorporation ratios were consistent with the relative levels of ER expressions in the cells.

Fluorescence imaging of the cells

Stable fluorescence images were obtained of the DESCIP incorporated cells (MCF-7, PC-3, and A-549) using green fluorescence of the DESCIP nanoparticles. Figure 8 shows fluorescence images of the cells. DESCIP presented significant fluorescence intensity on all cell lines (Fig. 8). For comparison, FITC commercial green fluorescence dye

labeled DESP were also incorporated into cells (Fig. 9). Fluorescein isothiocyanate (FITC) (3',6'-dihydroxyspiro[isobenzofuran-1(3H),9'-[9H]xanthen]-3-one) is a commercial dye molecule for fluorescent labeling. It binds to biomolecules substituting (-N=C=S group with hydrogen. FITC conjugated with DESP for comparison DESCIP fluorescent within the cells.

Cytotoxicity results

Four different concentrations (1, 2, 3, 4 ng/ml) were tested at 0 min, 24 h, 48 h, and 72 h of exposure. The 0 min value was chosen to confirm the viability of the cells. Cell viability above 80% was detected at 24, 48 and 72 h for all cell lines (MCF-7, PC-3, and A-549) for DESP and DESCIP. The results are given in Tables 4 and 5 for DESP and DESCIP, respectively.

Previously, Sharp et al. reported that 10–5 M, DES blocked the formation of microtubules in vitro [34]. Additionally, DES-induced apoptosis in androgen independent prostate cancer cell lines has also been reported independent from estrogen receptors [35, 36]. Finally, both DES monophosphate and diphosphate were cytotoxic on different malignant and transformed cell lines [37, 38].

In vivo scintigraphic imaging studies with rabbits

To evaluate the in vivo localization of ^{99m}Tc-DESCIP, scintigraphic images were taken after intradermal injection. Figure 10 shows static scintigrams of normal and receptor blocked female rabbits at several time intervals. Significant lymph node uptake dissimilarities were seen between normal and receptor blocked rabbits (Fig. 10). The uptake ratios were increased 3–4 between 1 h and 24 h imaging.

The sentinel lymph node is the first node that serves a cancer. It is exponentially more likely to contain a metastasis than a downstream, non-sentinel node. If one fails to identify sentinel lymph nodes that contain metastases, a physician is likely to incorrectly stage a cancer and inaccurately inform a patient that they are metastasis free.

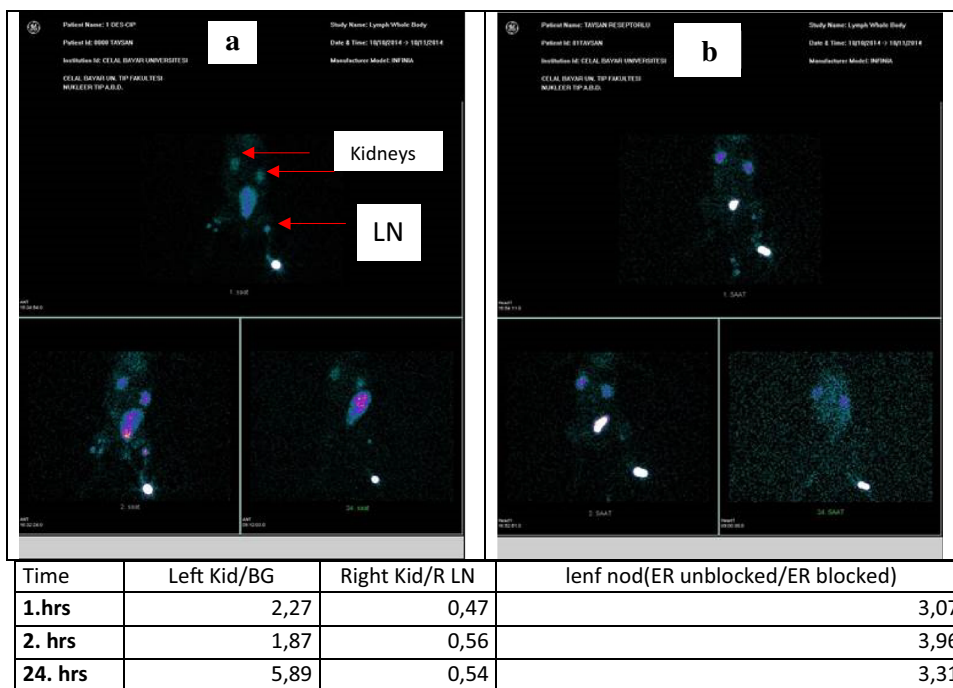
Multimodality imaging

There are many advantages to combining radionuclide imaging and FL imaging modalities into a multimodality imaging approach. Both PET/FL and SPECT/FL imaging involve the use of good, clinical contrast agents that lack toxicity and allow us to image disease at high spatial and longer temporal resolutions at trace quantities [39, 40]. The two modalities also complement each other in terms of spatial resolution at the histological and artificial level. Fluorescent probes are stable while the lifetime of radionuclide labeled probes depend on their half-life;

Table 5 Cellular cytotoxicity of DESCIP in 24, 48 and 72 h for MCF7, PC3 and A549 cells

24th h			
Log kons (ng/mL)	DES-CIP-MCF7	DES-CIP -PC3	DES-CIP -A549
0	93.22 ± 3.69	96.33 ± 3.21	95.5 ± 4.87
1	95.63 ± 4.21	93.29 ± 3.71	92.72 ± 3.56
2	93.45 ± 4.61	94.69 ± 4.79	95.59 ± 3.93
3	96.32 ± 3.88	92.56 ± 4.32	92.82 ± 2.97
4	94.39 ± 4.76	95.37 ± 4.57	93.98 ± 4.68
48th h			
Log kons (ng/mL)	DES-CIP -MCF7	DES-CIP -PC3	DES-CIP -A549
0	96.43 ± 3.32	94.51 ± 3.2	93.81 ± 4.11
1	97.32 ± 3.71	96.39 ± 3.88	95.32 ± 4.69
2	93.61 ± 3.99	92.89 ± 4.59	97.38 ± 3.87
3	94.29 ± 4.29	94.88 ± 4.34	94.22 ± 3.18
4	96.39 ± 4.55	95.25 ± 3.52	95.43 ± 4.45
72th h			
Log kons (ng/mL)	MCF7	PC3	A549
0	94.23 ± 2.54	97.74 ± 3.52	95.36 ± 3.11
1	96.29 ± 5.28	95.42 ± 4.82	96.24 ± 4.21
2	91.8 ± 4.82	98.63 ± 4.26	92.77 ± 2.34
3	93.67 ± 3.72	92.39 ± 3.75	93.33 ± 4.78
4	94.27 ± 3.31	96.59 ± 2.59	97.46 ± 4.32

Fig. 10 Scintigraphic images of female rabbits: **a** receptor unblocked, and **b** receptor blocked



however, radionuclide labeled probes are superior to FL for their efficacy in providing non-invasive, high resolution visualization of cell and tissue structure through deep

tissue. Therefore, multimodality radionuclide/FL probes are superior to standalone SPECT/PET and FL contrast agents.

In many cancers, a primary tumor is easily resected and not a cause for concern. Cancer metastasis, however, can be lethal. For this reason, it is vitally important to accurately identify the presence of metastasis following diagnosis of cancer. Lymph node imaging is important to determine if metastasis exists or not. Metastasis is easily observed non-invasively in ^{18}F -FDG-PET scans. Unfortunately, ^{18}F -FDG-PET scans only indicate metabolism and do not provide biomarker or morphological information that an oncologist could use in determining appropriate drugs for treating a cancer. Because of this, it is vital to isolate and biopsy the lymph nodes that serve a cancer, even in patients who receive ^{18}F -FDG-PET scans. This is especially true in breast, melanoma, and squamous cell carcinoma of the oral cavity.

The results showed that DESCIP nanoparticles can be radiolabeled with $^{99\text{m}}\text{Tc}$ in high yields. It may potentially be proposed as multifunctional probe both for SPECT and optical for estrogen receptor targeting.

Conclusion

DESCIP (DES containing nanoparticles) demonstrates both fluorescence capability and ER receptor targeting specificity. Nanostructured fluorescence property was successfully conferred, and desirable particle size and zeta potential values were obtained. DESCIP was also successfully radiolabeled with $^{99\text{m}}\text{Tc}$. Biological behavior and ER targeting capability was determined by in vivo and in vitro studies. Results indicate that DESCIP may be beneficial for detecting estrogen-overexpressed tissues in animal models.

DESCIP improves the effects of DES and may be a novel and important means of increasing theranostic efficacy of cytotoxic chemotherapy and imaging agents.

References

1. Dodds EC, Goldberg L, Larson W, Robinson R (1938) Estrogenic activity of certain synthetic compounds. *Nature* 141:247–248
2. Turo R, Smolski M, Esler R, Kujawa ML, Bromage SJ, Oakley N, Adeyoju A, Brown SCW, Brough R, Sinclair A, Collins GN (2014) Diethylstilboestrol for the treatment of prostate cancer: past, present and future. *Scand J Urol* 48:4–14
3. Benninka HJTC, Verhoevena C, Dutmana AE, Thijssenb J (2017) The use of high-dose estrogens for the treatment of breast cancer. *Maturitas* 95:11–23
4. de Vries Schultink AH, Alexi X, van Werkhoven E, Madlensky L, Natarajan L, Flatt SW, Zwart W, Linn SC, Parker BA, Wu AH, Pierce JP, Huitema AD, Beijnen JH (2017) An antiestrogenic activity score for tamoxifen and its metabolites is associated with breast cancer outcome. *Breast Cancer Res Treat* 161:567–574
5. Muftuler FZB, Unak P, Teksoz S, Acar C, Yolcular S, Yurekli Y (2008) I-131 labeling of tamoxifen and biodistribution studies in rats. *Appl Radiat Isot* 66:178–187
6. Palmieri C, Cheng GJ, Saji S, Zelada-Hedman M, Wärrri A, Weihua Z, Van Noorden S, Wahlstrom T, Coombes RC, Warner M, Gustafsson JÅ (2002) Estrogen receptor beta in breast cancer. *Endocr Relat Cancer* 9(1):1–13
7. Gross JM, Yee D (2002) How does the estrogen receptor work? *Breast Cancer Res* 4:62–64
8. Strickland LA, Ponce YZ, Hunter DH, Zabel PL, Powe JE, Morrisey G, Driedger AA, Chamberlain MJ (1990) Amino and iodotamoxifens: synthesis estrogen receptor affinity and biodistribution. *Drug Des Deliv* 6:195–212
9. Skaddan MB, Wust FR, Jonson S, Syhre R, Welch JM, Spies H, Katzenellenbogen JA (2000) Radiochemical synthesis and tissue distribution of Tc-99m-Labeled 7α -substituted estradiol complexes. *Nucl Med Biol* 27:269–778
10. Van DeWiele C, De Vos F, Slegers G, Van Belle S, Dierckx RA (2000) Radiolabelled estradiol derivatives to predict response to hormonal treatment in breast cancer: a review. *Eur J Nucl Med* 27:1421–1433
11. Unak P, Muftuler FZB, Ichedef C, Medine IE, Ozmen K, Unak T, Yurt Kilcar A, Gumuser FG, Parlak Y, Bilgin ES (2012) Synthesis, radiolabeling and in vivo biodistribution of diethylstilbestrol phosphate derivative (DES-P). *J Radioanal Nucl Chem* 293:57–66
12. Droz JP, Kattan J, Bonnay M, Chraïbi Y, Bekradda M, Culine S (1993) High-Dose continuous-infusion fofestrol in hormone-resistant prostate cancer. *Cancer* 71:1123–1130
13. Ertay T, Unak P, Ozdogan O, Biber FZ, Zihnioglu F, Medine EI, Durak H (2006) Tc-99 m-exorphan-glucuronide in tumor diagnosis: preparation and biodistribution studies in rats. *J Radioanal Nucl Chem* 269:21–28
14. Guldu OK, Unak P, Medine E, Barlas FB, Muftuler FZB, Timur S (2015) Radioiodinated magnetic nanoparticles conjugated with moxifloxacin: synthesis and in vitro biological affinities. *Int J Polym Mater* 64:253–259
15. Sanders JE, Chuang A, Swiec GD, Bisch FC, Herold RW, Buxton TB, McPherson JC (2011) The effects of enamel matrix derivative and cyclic mechanical strain on human gingival fibroblasts in an in vitro defect healing model. *Int J Periodontics Restor Dent* 31:671–678
16. Bordoloi JK, Berry D, Khan IU, Sunasseea K, de Rosales RTM, Shanahan C, Blower PJ (2015) Technetium-99 m and rhenium-188 complexes with one and two pendant bisphosphonate groups for imaging arterial calcification. *Dalton Trans* 44:4963–4975
17. Kuiper GGJM, Enmark E, PelttoHuikko M, Nilsson S, Gustafsson JA (1996) Cloning of a novel estrogen receptor expressed in rat prostate and ovary. *Proc Natl Acad Sci USA* 93:5925–5930
18. Ogawa S, Inoue S, Watanabe T, Hiroi H, Orimo A, Hosoi T, Ouchi Y, Muramatsu M (1998) The complete primary structure of human estrogen receptor beta (hER beta) and its heterodimerization with ER alpha in vivo and in vitro. *Biochem Biophys Res Comm* 243:122–126
19. Piccolella M, Crippa V, Messi E, Tetel MJ, Poletti A (2014) Modulators of estrogen receptor inhibit proliferation and migration of prostate cancer cells. *Pharmacol Res* 79:13–20
20. Omoto Y, Eguchi H, Yamamoto-Yamaguchi Y, Hayashi S (2003) Estrogen receptor (ER) β 1 and ERbcx/ β 2 inhibit ER α function differently in breast cancer cell line MCF7. *Oncogene* 22:5011–5020
21. Leav I, Sm Ho, Ofner P, Fb Merk, Pwl Kwan, Damassa D (1988) Biochemical alterations in sex hormone-induced hyperplasia and dysplasia of the dorsolateral prostates of Noble rats. *J Nat Cancer Inst* 80:1045–1053

22. Bianco JJ, Handelsman DJ, Pedersen JS, Risbridger GP (2002) Direct response of the murine prostate gland and seminal vesicles to estradiol. *Endocrinology* 143:4922–4933
23. McPherson SJ, Wang H, Jones ME, Pedersen J, Iismaa TP, Wreford N, Simpson ER, Risbridger GP (2001) Elevated androgens and prolactin in aromatase-deficient mice cause enlargement, but not malignancy, of the prostate gland. *Endocrinology* 142:2458–2467
24. Royuela M, de Miguel MP, Bethencourt FR, Sanchez-Chapado M, Fraile B, Arenas MI, Paniagua R (2001) Estrogen receptors alpha and beta in the normal, hyperplastic and carcinomatous human prostate. *J Endocrinol* 168:447–454
25. Da J, Lu MJ, Wang Z (2015) Estrogen receptor alpha (ER α)-associated fibroblasts promote cell growth in prostate cancer. *Cell Biochem Biophys* 73:793–798
26. Royuela M, de Miguel MP, Bethencourt FR, Sanchez-Chapado M, Fraile B, Arenas MI, Paniagua R (2001) Estrogen receptors alpha and beta in the normal, hyperplastic and carcinomatous human prostate. *J Endocrinol* 168:447–454
27. Bonkhoff H, Fixemer T, Hunsicker I, Remberger K (1999) Estrogen receptor expression in prostate cancer and premalignant prostatic lesions. *Int J Periodontics Restor Dent* 155:641–647
28. Mobbs BG, Johnson IE, Liu Y (1990) Quantitation of cytosolic and nuclear estrogen and progesterone receptor in benign, untreated, and treated malignant human prostatic tissue by radioligand binding and enzyme-immunoassays. *Prostate* 16:235–244
29. Bonkhoff H, Berges R (2009) The evolving role of oestrogens and their receptors in the development and progression of prostate cancer. *Eur Urol* 55:533–542
30. Ricke WA, McPherson SJ, Bianco JJ, Cunha GR, Wang Y, Risbridger GP (2008) Prostatic hormonal carcinogenesis is mediated by in situ estrogen production and estrogen receptor alpha signaling. *FASEB Journal* 22:1512–1520
31. Couse JF, Lindzey J, Grandien K, Gustafsson JA, Korach KS (1997) Tissue distribution and quantitative analysis of estrogen receptor-alpha (ERalpha) and estrogen receptor-beta (ERbeta) messenger ribonucleic acid in the wild-type and ERalpha-knockout mouse. *Endocrinology* 138:4613–4621
32. Raso MG, Behrens C, Herynk MH, Liu SY, Prudkin L, Czburn NC, Woods DM, Tang XM, Mehran RJ, Moran C, Lee JJ, Wistuba II (2009) Immunohistochemical expression of estrogen and progesterone receptors identifies a subset of NSCLCs and correlates with EGFR mutation. *Clin Cancer Res* 15:5359–5368
33. Abe K, Miki Y, Ono K, Mori M, Kakinuma H, Kou Y, Kudo N, Koguchi M, Niikawa H, Suzuki S, Evans DB, Sugawara S, Suzuki T, Sasano H (2010) Highly concordant coexpression of aromatase and estrogen receptor beta in non-small cell lung cancer. *Hum Pathol* 41:190–198
34. Sharp DC, Parry JM (1985) Diethylstilboestrol: the binding and effects of diethylstilboestrol upon the polymerisation and depolymerisation of purified microtubule protein in vitro. *Carcinogenesis* 6:865–871
35. Robertson CN, Roberson KM, Padilla GM, O'Brien ET, Cook JM, Kim CS, Fine RL (1996) Induction of apoptosis by diethylstilbestrol in hormone-insensitive prostate cancer cells. *J Natl Cancer Inst* 88:908–917
36. Montgomery RB, Bonham M, Nelson PS, Grim J, Makary E, Vessella R, Stahl WL (2005) Estrogen effects on tubulin expression and taxane mediated cytotoxicity in prostate cancer cells. *Prostate* 65:141–150
37. Schulz P, Vetter I, Bauer HW, Fittler F (1988) Evaluation of the cytotoxic activity of diethylstilbestrol and its phosphorylated derivatives towards prostatic carcinoma, non prostatic neoplastic and non-transformed cells. *Urol Itit* 43(Suppl 1):5–9
38. Schneider MR, Schonenberger H (1988) Effects of diethylstilbestrol and its mono- and diphosphate on experimental mammary and prostatic tumors. *Urol Itit* 43(Suppl 1):10–4
39. Tsien RY (2003) Imagining imaging's future. *Nat Rev Mol Cell Biol* 4:16–21
40. Nguyen QT, Tsien RY (2013) Fluorescence-guided surgery with live molecular navigation—a new cutting edge. *Nat Rev Cancer* 13:653–662